PHYSICAL REVIEW B VOLUME 20, NUMBER 10 15 NOVEMBER 1979

Energy dependence of 3*d*, 4*d*, 5*d*, and 4*f* photoionization partial cross sections

L. I. Johansson, I. Lindau, and M. Hecht
Stanford Synchrotron Radiation Laboratory, Stanford University, Stanford, California 94305

S. M. Goldberg and C. S. Fadley
Department of Chemistry, University of Hawaii, Honolulu, Hawaii 96822
(Received 9 January 1979)

The photoionization partial cross sections of the Ga 3*d*, As 3*d*, Sb 4*d*, Pb 5*d*, Au 5*d*, and Au 4*f* subshells have been mapped out from threshold and up to a few hundred eV above threshold by means of the photoemission technique. The experiments were performed on solids using synchrotron radiation, in the photon energy range 40–700 eV, as an excitation source. Atomic partial photoionization cross sections were calculated using the Herman-Skillman central-potential model (HS approximation). The calculated energy dependence for the atomic case is compared to the experimentally determined energy dependence in the solid phase.

INTRODUCTION

Partitioning of total photoionization cross sections into the individual subshell contributions σ_{nl} and determination of the energy dependence of those partial cross sections is of importance for many applications.[1-5] One of the most direct methods for obtaining such information is by the photoemission technique. By using this technique with a tunable light source, we have been able to map out in detail the behavior of various subshell cross sections from threshold and up to several hundred eV above threshold.

We have employed this technique on solids for studying the energy dependence of a few 3*d*, 4*d*, 5*d*, and 4*f* differential cross sections. To date, most of the experimental work on cross sections has been done in the gas phase in order to approach more closely the atomic case which is considered by theoretical models.[1-3,6,7] However, accumulation of cross-section data for solids is also of great interest, not the least for determining in detail the differences between the gas and the solid phase in order to improve our understanding of the effect of the solid-state environment on electron correlation effects.

Below we present our experimental results on solids and calculated atomic values and discuss them within the one-electron model. Our results are compared to previous experimental results on solids[8-10] and to other calculations.[6,7]

I. ATOMIC-CROSS-SECTION CALCULATION

The photoelectrons ejected from a collection of randomly oriented atoms, upon photoionization with plane polarized light, get an angular distribution described[11] by

$$\frac{d\sigma_{nl}}{d\Omega} = \frac{\sigma_{nl}}{4\pi}\left(1 + \frac{\beta_{nl}}{2}(3\cos^2\theta - 1)\right), \tag{1}$$

where σ_{nl} is the partial cross section, β_{nl} the asymmetry parameter, and θ the angle between photon electric vector and photoelectron direction. The partial cross section is in the dipole approximation given[6] by

$$\sigma_{nl}(E) = \frac{4\pi^2\alpha a_0^2}{3}\frac{(E - E_{nl})N_{nl}}{2l+1}\left[lR^2_{E,l-1} + (l+1)R^2_{E,l+1}\right],$$

where α is the fine-structure constant, a_0 the Bohr radius, N_{nl} the number of electrons in the nl subshell, E_{nl} the binding energy, and E the kinetic energy of the ejected electron, defined so that $h\nu = E - E_{nl}$ represents the energy of the incident photon. The radial dipole matrix elements are

$$R_{E,l\pm1} = \int_0^\infty P_{nl}(r) r P_{E,l\pm1}(r)\, dr,$$

where $P_{nl}(r)/r$ and $P_{E,l\pm1}(r)/r$ are the radial parts of the single-particle wave functions of, respectively, the initial and final state. The asymmetry parameter $\beta_{nl}(E)$ is determined[6,11] by the radial dipole matrix elements and the phase shift in the final continuum state wave function. For photon energies well above threshold usually the $R_{E,l+1}$ matrix element is so much larger than the $R_{E,l-1}$ element that it essentially[12] determines the energy dependence.

We have calculated[13] partial photoionization cross sections and asymmetry parameters using the Herman-Skillman (HS) central potential model.[2] The calculated values are compared to the experimental results obtained on solids. Since our data were collected with an analyzer that has a large-acceptance solid angle, Eq. (1) for example can-

not be applied directly. The average differential cross section[14] for our experimental geometry was therefore calculated and found to be

$$\left\langle \frac{d\sigma_{nl}}{d\Omega'} \right\rangle_{av} = \left(\int_{\Omega'} \frac{d\sigma_{nl}}{d\Omega} d\Omega \right) \Big/ \Omega' = \frac{\sigma_{nl}}{4\pi}(1 + \beta_{nl} \times 0.288) , \tag{2}$$

where Ω' is the acceptance solid angle of the analyzer. This expression has been used in the comparison of calculated and experimental results. The applicability of an average differential cross section for analyzers with large acceptance solid angles has been questioned,[14,15] but it constitutes the best choice for our experimental geometry.

II. EXPERIMENTAL

The experiments were performed on the 4° line of Beam Line I at Stanford Synchrotron Radiation Laboratory. Monochromatized radiation from the grazing incidence "grasshopper" monochromator[16] was used for photoexcitation. The emitted electrons were energy analyzed in a double pass cylindrical mirror analyzer which has an energy resolution of 1.6%, relative to the analyzer pass energy.[17] The analyzer was operating in the retarding mode, thus at a fixed pass energy. A pass energy of 100 eV was normally chosen in order to obtain short recording times. The analyzer was located so that its optical axis was laying in the incidence plane of the plane-polarized radiation but at an angle of 75° relative to the incidence direction. The samples were positioned in such a way that the surface normal coincided (within a few degrees) with the optical axis of the analyzer. Thus the results presented below represent angular integrated data, integrated over polar angles between 36° and 48°.

The samples used were either *in situ* cleaved semiconductor crystals (GaAs and GaSb) or *in situ* prepared films (Au and Pb), by evaporation onto a stainless steel substrate. The instrument used was operated under ultrahigh vacuum conditions, $\leq 2 \times 10^{-10}$ Torr.

Cross-section measurements using photoemission are in principle very straightforward. By measuring the intensity of a photoelectron peak (the peak area)[18] one deduces the relative differential cross section simply by normalizing out the incident photon flux and the analyzer efficiency. However, the photon flux out at the grasshopper monochromator varies not only with energy but also with time, especially at high photon energies, since a gradual carbon buildup on the optical elements degrades the performance of the monochromator. Thus care must be taken for making a proper normalization.

The photon flux in the energy range 40–250 eV was measured using a calibrated (NBS photodiode)[19] (Al_2O_3 diode). In order to frequently monitor the relative photon flux and to determine the relative flux above 250 eV the electron yield from gold films was measured before and after the cross-section measurements. By dividing the electron yield with the absorption coefficient[20] a measure[21] of the relative photon flux is obtained (see Fig. 1). In the energy range 140–250 eV the NBS diode and gold-yield results correlated very well, but between 40 and ~130 eV the NBS diode gave a significantly higher relative flux (see inset in Fig. 1). This difference at the low photon energies (which probably[21] is due to the steep increase in the absorption coefficient of gold when going from 130 to 30 eV) has been corrected for in all flux determinations from gold-yield measurements. No correction for scattered light and second-order radiation has been made.

After establishing the energy dependence of the relative photon flux prior to the cross-section measurements we relied on the stability of the SPEAR storage ring (Stanford's electron-positron storage ring) for the actual flux during the experiment. Experience has shown that it can be assumed to be proportional to the stored beam current.

The analyzer efficiency has been predicted[17] to

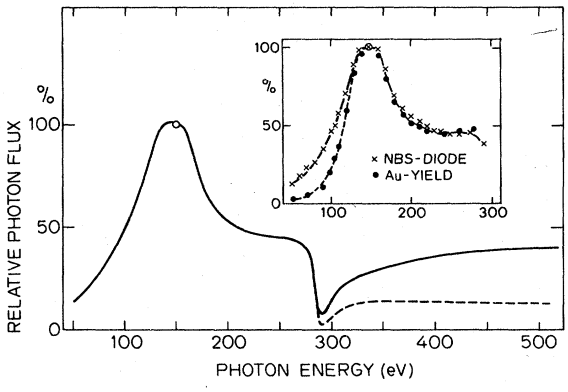

FIG. 1. Relative photon flux (solid line) from the "grasshopper" monochromator as determined from electron yield measurements on gold. Photon flux is highest around 150 eV and we have therefore arbitrarily chosen 150 eV as the normalization point between different measurements. Deterioration in performance with time of the monochromator is illustrated by the dashed line, which represents results obtained in a measurement two months later. Data are corrected for the difference observed in the relative photon flux, between 40 and 130 eV, as determined from gold-yield and NBS-diode measurements (see inset).

vary as E_p/E_{kin} when operated in the retarding mode,[22] where E_p represents the analyzer pass energy and E_{kin} the kinetic energy of the analyzed electron. This introduces a large correction factor in our case because we kept E_p typically at 100 eV and analyzed electrons with kinetic energies between about ten and a few hundred eV. Ideally one would like to have the analyzer efficiency calibrated for the specific application, but since this is not yet available we have to rely on the theoretical prediction. We have, though, for the 3*d*'s of GaAs obtained essentially identical results on the energy dependence of the cross section when using pass energies of 15, 25, 50, and 100 eV.

III. RESULTS

Energy distribution curves of photoelectrons emitted from a GaSb crystal are shown in Fig. 2 for three different photon energies. The peak at about 20 eV electron binding energy is the Ga-3*d* photoelectron peak while the one around 33 eV is due to Sb-4*d* electrons. The relative amplitudes of the 3*d* and 4*d* peaks are seen to vary drastically with changing photon energy. This is due to a strong energy dependence of the partial photoionization cross section for the 4*d* electrons. The figure makes visual the importance of having knowledge about this energy dependence when selecting a suitable photon energy for studying a particular subshell, i.e., for tuning the sensitivity in an experiment.

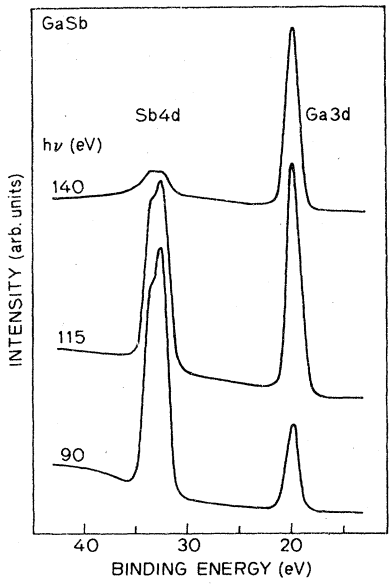

FIG. 2. Electron energy distributions from GaSb for three different excitation energies. Binding energies are referred to the Fermi level. The drastic variation in 3*d* to 4*d* photoelectron intensity ratio is due to a strong energy dependence in the cross section for 4*d* photoionization.

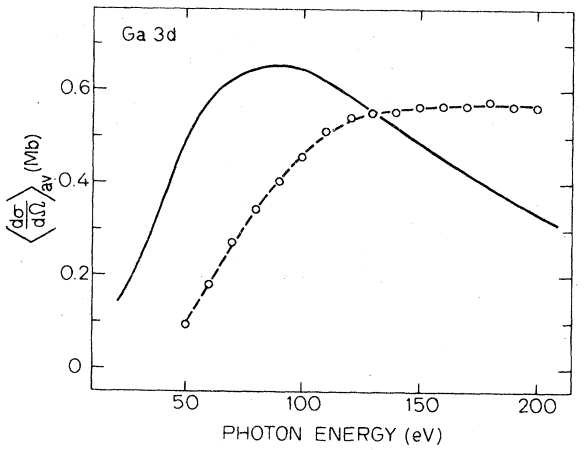

FIG. 3. Differential cross section for Ga 3*d*. Solid curve represents values calculated in the HS central-field approximation. Circles represent experimental results (on GaAs) corrected for relative photon flux and analyzer efficiency. Experimental results obtained at 130 eV are fitted to the calculated value.

The 3*d* cross section has a rather smooth and weak energy dependence as shown in Figs. 3–5. The Ga-3*d*, As-3*d* and Kr-3*d* calculated differential cross sections all show an increase with energy from onset up to a broad maximum at about 80 eV above threshold. Above the maximum the cross sections decrease monotonically with energy. The experimental results shown in Figs. 3 and 4 have been fitted to the calculated values at points indicated in the figures since we cannot assess absolute cross-section values from our experi-

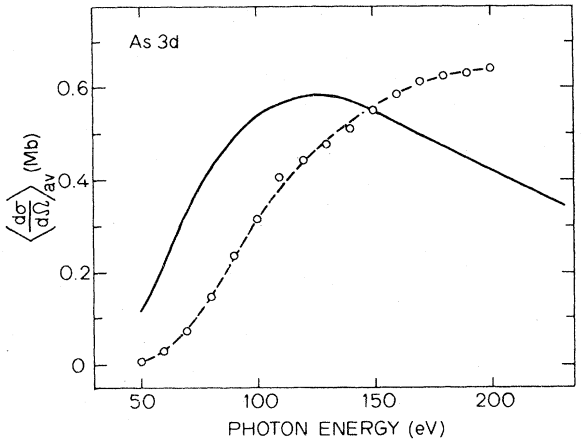

FIG. 4. Differential cross section for As 3*d*. Experimental results obtained (on GaAs) at 150 eV photon energy are fitted to the calculated value.

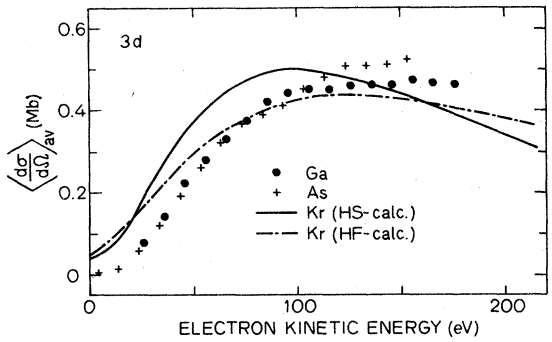

FIG. 5. Comparison of calculated differential cross sections for Kr 3*d* with experimental results on Ga 3*d* and As 3*d*. Dash-dot curve represents values calculated by Kennedy and Manson (Ref. 6) in the HF length approximation. Experimental results are fitted to a value of 0.45 Mb at about 105-eV electron kinetic energy. Binding energies (referred to the vacuum level) used for assessing kinetic energies are 24.5, 46.5, and 89 eV for Ga 3*d*, As 3*d*, and Kr 3*d* respectively.

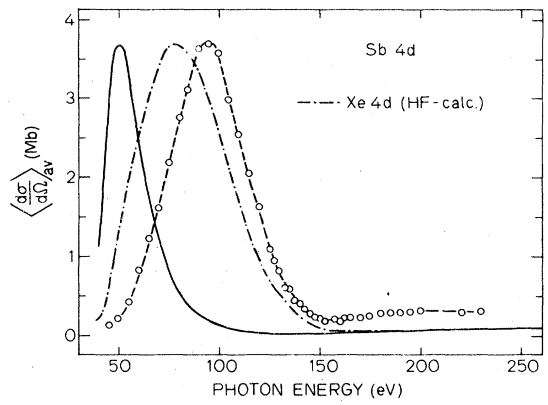

FIG. 6. Differential cross section for Sb 4*d*. Dash-dot curve represents values for Xe 4*d* calculated by Kennedy and Manson (Ref. 6) in the HF length approximation. Experimental results and the calculated Xe-4*d* HF values are fitted so that their maximum values coincide with the maximum value calculated for Sb 4*d* in the HS approximation.

ment.

The energy dependence of the 3*d* cross section can qualitatively be understood by considering the dominant $l+1$ channel, i.e., $3d \rightarrow \epsilon f$ transitions. At low photon energies the continuum *f* orbital lies essentially outside the region of space occupied by the bound 3*d* orbital, so the radial matrix element is small. As the energy is increased the maximum of the continuum orbital moves closer to the nucleus and the overlap and thus the dipole matrix element increases. A maximum occurs when maximum overlap is obtained and thereafter the matrix element decreases monotonically as the continuum orbital moves further in towards the nucleus.

For Ga 3*d* and As 3*d* we see Figs. 3 and 4 that the calculated (solid line) and experimental (dashed line) results deviate significantly. The experimental results show a slower increase with energy from onset and the broad maxima is located considerably higher up in energy than the calculation predicts. The fitting of the measured values to the calculated ones has been made at points that nearly coincide if the differential cross sections are plotted versus electron kinetic energy as shown in Fig. 5. There, a comparison to calculated values for Kr 3*d* is made. Included in the figure are also values calculated by Kennedy and Manson[6] in the Hartree-Fock (HF) approximation (dash-dot line). The trend with energy in our Ga-3*d* and As-3*d* data follows the trend of the calculated Kr-3*d* differential cross section rather well; this has been observed previously.[23]

The 4*d* differential cross section should have a much more dramatic energy dependence than was the case for 3*d*'s because 4*d* radial wave functions have nodes and the cross sections should thus exhibit Cooper minima.[12] This can also be qualitatively understood by considering the dominant $l+1$ channel. At electron kinetic energies for which the maximum in the continuum *f* orbital starts to overlap the node of the bound 4*d* orbital, the radial dipole matrix element begins to decrease and with increasing energy it actually changes sign, thus giving rise to a minimum, a Cooper minimum, in the cross section. In Fig. 6 calculated and experimental results are shown for Sb 4*d*. The cross section is seen to increase rapidly with energy from onset up to a sharp maximum. It then decreases rapidly, passes through a broad minimum (the Cooper minimum), increases again but slowly, and passes through a broad second maximum, whereafter it decreases monotonically with increasing energy. The calculated values for Sb 4*d* predict the general trends observed experimentally but are off regarding the actual location of especially the first sharp maximum, as seen in Fig. 6. Also included in the figures are values for Xe 4*d* calculated by Kennedy and Manson[6] in the HF approximation (dash-dot curve). Again the HF calculation for the rare gas describes the observed energy dependence of the Sb-4*d* cross section rather well, as observed previously.[8] However, such detailed agreement as was claimed previously between the calculated Xe-4*d* and experimental Sb-4*d* cross sections is not obtained. A binding energy (referred to the vacuum level) of 37.5 eV was used for the Sb 4*d* level in GaSb in assigning the threshold energy for photoionization.

The 5*d* differential cross section of Pb also ex-

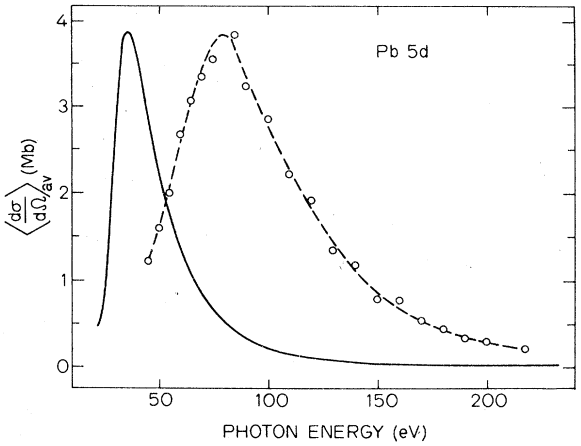

FIG. 7. Differential cross section in Pb 5*d*. Experimental results are fitted so that the maximum value coincides with the calculated maximum value.

hibits a rather dramatic energy dependence, as shown in Fig. 7. The calculation again predicts the maximum to be closer to threshold than what is observed experimentally but it gives the general trend of the energy dependence. A rapid increase from threshold and up to a sharp maximum and thereafter a monotonic decrease with increasing energy. In Fig. 8 the Au-5*d* differential cross section is shown for photon energies above 60 eV. A monotonic decrease with energy is observed only since the photon energies are too high to see the maximum, which is located less than 30 eV above threshold according to previous results.[10] Our data agree reasonably well with the previously presented results[10] for the Au-5*d* valence-band intensity.

Electrons from levels with higher angular momenta (such as 4*f* electrons) have a larger "repulsive barrier" to overcome[1,2,6] upon photoexcitation before escaping into vacuum than electrons from levels with lower angular momenta have. Due to this the 4*f* partial cross section should show[1,2,6] a slow onset at the threshold and the maximum should fall relatively high up in energy. The delayed onset of the Au-4*f* differential cross section is seen clearly both in the calculated and experimental results, shown in Fig. 9. The maximum in cross section occurs approximately 200 eV above threshold and thereafter the cross section decreases monotonically towards higher energies. The overall trend is predicted well by the atomic model in this case and our results are in agreement with earlier observations[9] on the Au 4*f* subshell, which were performed over a much narrower energy range.

IV. DISCUSSION

In Sec. III experimentally determined relative partial cross sections on solids were compared to values calculated within the HS central potential model for atoms. A good quantitative agreement was not expected to be obtained since electron correlation effects are not included in this model.[1,2,6,7] These effects are particularly important close to threshold because the outgoing electrons then travel slowly and have ample time to interact strongly with the rest of the electrons in the solid. The atomic HS central-potential model is thus not expected to give an accurate prediction of the detailed behavior of the partial cross section close to threshold but it constitutes a reasonably good starting point for interpreting the cross-section energy dependence. Our comparison should thus be seen as an attempt to elucidate how much this model can aid in the interpretation of data on solids and to what accuracy.

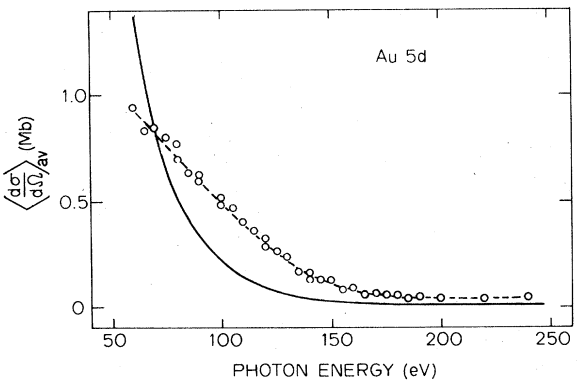

FIG. 8. Differential cross sections for Au 5*d* (valence band). Experimental results obtained at 70 eV are fitted to the calculated value.

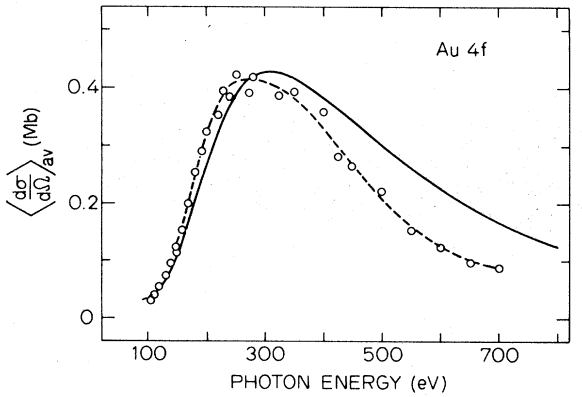

FIG. 9. Differential cross sections for Au 4*f*. Experimental results are fitted so that the maximum value coincides with the calculated maximum value.

If final-state correlations are included in the calculation of 4d- and 5d-subshell cross sections, it has been shown[7] that the oscillator strength is redistributed in such a way that the position of the cross-section maxima is raised in energy and flattened out for the materials we have studied. In HF calculations electron correlation effects are taken into account, which means that such calculations should predict better the cross-section behavior close to threshold. So far HF calculations have been carried out only for rare gases, which explains why we compare our experimental results with HF-calculated values only for Kr 3d and Xe 4d. For Kr 3d the HF calculation, compared to the HS calculation, actually does flatten out the maximum and push it up in energy, as seen in Fig. 5. The energy dependence of the Kr-3d cross section describes rather well the observed behavior for Ga 3d and As 3d. The Xe-4d HF values describe to about the same accuracy the energy dependence of the Sb-4d cross section although the location of the maxima differ by about 15 eV. This is, however, reasonable since the trend obtained by Combet-Farnoux[7] with atomic number when including final-state correlations in the calculation indicates that the maximum should be located slightly higher above threshold for Sb ($Z=51$) than for Xe ($Z=54$).

For the 5d subshell Combet-Farnoux's[7] calculation indicates that the correlation effect pushes the cross-section maximum to about 10–15 eV higher energy (for $79 \leq Z \leq 83$) than what the HS calculation predicts. This, however, does not resolve the discrepancy seen for Pb 5d in Fig. 7. In the case of Au 5d the atomic calculation is expected to give a less good description of the solid phase since the Au-5d electrons constitute the valence band in the solid, so the radial wave functions should differ considerably from the atom.

For the Au 4f subshell, the situation regarding the location of the cross-section maximum is reversed. In this case the HS values locate the maximum higher in energy than what is observed experimentally. Maybe crystal field effects in the solid tend to decrease the repulsive barrier, which should mean that an atomic calculation overestimates its importance.

In the extraction of the experimental data, we have neglected effects than can be of importance if one tries to do a more detailed comparison. The probing depth, for example, varies with kinetic energy since the electron escape depth[24] is energy dependent, and for low kinetic energies electron refraction effects at the surface become important.[14] At lower kinetic energies, however, these effects partially cancel each other. That is the reason why in the present discussion we felt justified in neglecting these effects, since most of our data cover the low kinetic energy range. One should be aware, though, that this means that we overestimate the cross section at high kinetic energies for Au 4f, since a larger energy range is covered in this case.

Finally we want to emphasize that in the present discussion we have deliberately restricted ourselves to the single-electron model and consequently have not mentioned multielectron effects (such as plasmons, shake-ups, and collective resonances) that fall outside the one-electron picture. Multielectron effects can be of major importance for certain materials,[3,4,25,26] but we believe that the one-electron model gives a reasonably good description for the cases presented above.

V. SUMMARY

We have presented experimental and calculated results on the energy dependence of some 3d-, 4d-, 5d-, and 4f-subshell cross sections. The experiments were performed on solids while the calculations, made in the HS central potential model, describe the atomic case. The calculated values describe rather well the general form of the energy dependence for the cases presented but locate the maxima of the 3d, 4d, and 5d cross sections much closer to threshold than what is observed experimentally. This can be attributed mainly to the neglect of electron correlation effects in the HS model, although Combet-Farnoux's calculation in which final-state correlations were included does not push the maxima high enough above the threshold to give a really good fit to our data. However, HF calculations for the rare-gas subshells Kr 3d and Xe 4d describe fairly well the energy dependence of the Ga 3d and Sb 4d levels studied.

For the Au 4f subshell the HS model locates the cross-section maximum at higher energy than what is observed experimentally. The general shape though is well reproduced.

The discrepancies observed in our work between calculated atomic values and experimental results on solids can hopefully initiate future refined calculations to elucidate the importance of correlation effects in solids.

ACKNOWLEDGMENTS

We wish to thank Dr. P. Pianetta for his help in carrying out the experiments. This work was supported by the National Science Foundation under Contract No. DMR 77-02519. The experiments were performed at the Stanford Synchrotron Radiation Laboratory, which is supported by the National Science Foundation under Contract No. DMR 77-27489 in cooperation with the Stanford Linear Accelerator Center and the Department of Energy.

[1]U. Fano and J. W. Cooper, Rev. Mod. Phys. 40, 441 (1968).
[2]S. T. Manson and J. W. Cooper, Phys. Rev. 165, 126 (1968); 177, 157 (1969).
[3]M. Ya. Amusia and N. A. Cherekov, Case Stud. At. Phys. 5, 47 (1975).
[4]*Photoionization and Other Probes of Many Electron Interactions*, edited by F. J. Wuilleumier (Plenum, New York, 1976).
[5]V. I. Nefedov and V. G. Yarzhemsky, J. Electron Spectrosc. Relat. Phenom. 11, 1 (1977), and references therein.
[6]D. J. Kennedy and S. T. Manson, Phys. Rev. A 5, 227 (1972).
[7]F. Combet-Farnoux, in *Proceedings of the International Conference on Inner Shell Ionization Phenomena, Atlanta, 1972* (U.S. AEC, Oak Ridge, 1973), Vol. 2, p. 1130.
[8]I. Lindau, P. Pianetta, and W. E. Spicer, Phys. Lett. A 57, 225 (1976).
[9]I. Lindau, P. Pianetta, K. Y. Yu, and W. E. Spicer, Phys. Rev. B 13, 492 (1976).
[10]J. Stöhr, G. Apai, P. S. Wehner, F. R. McFeely, R. S. Williams, and D. A. Shirley, Phys. Rev. B 14, 5144 (1976).
[11]J. Cooper and R. N. Zare, in *Lectures on Theoretical Physics*, edited by S. Geltman, K. Mahanthappa, and W. Brittin (Gordon and Breach, New York, 1969), Vol. 11-C, p. 317.
[12]J. W. Cooper, Phys. Rev. 128, 681 (1962).
[13]S. T. Manson has kindly supplied us with a program for calculating photoionization cross sections in the HS approximation.
[14]C. S. Fadley, Prog. Solid-State Chemistry 11, 265 (1976).
[15]M. P. Seah, Surf. Sci. 32, 703 (1972).
[16]F. C. Brown, R. Z. Bachrach, and N. Lien, Nucl. Instrum. Methods 152, 73 (1978).
[17]P. W. Palmberg, J. Vac. Sci. Technol. 12, 379 (1975).
[18]P. R. Woodruff, L. Torop, and J. B. West, J. Electron Spectrosc. Relat. Phenom. 12, 133 (1977).
[19]E. B. Saloman and D. L. Ederer, Appl. Opt. 14, 1029 (1975).
[20]H.-J. Hagemann, W. Gudat, and C. Kunz, J. Opt. Soc. Am. 65, 742 (1975).
[21]W. Gudat, Internal Report No. DESY F41-74/10 (unpublished).
[22]This relation has been tested experimentally at Physical Electronics Industries Inc. according to P. W. Palmberg (private communication), but the results have not been published.
[23]I. Lindau, P. Pianetta, and W. E. Spicer, in Proceedings of the International Conference on the Physics of X-ray Spectra, Gaithersburg, 1976 (unpublished).
[24]I. Lindau and W. E. Spicer, J. Electron Spectrosc. Relat. Phenom. 3, 409 (1974).
[25]L. I. Johansson, J. W. Allen, T. Gustafsson, I. Lindau, and S. B. M. Hagstrom, Solid State Commun. 28, 53 (1978).
[26]M Hecht, I. Lindau, and L. I. Johansson, Jpn. J. Appl. Phys. Suppl. 17-2, 249 (1978).